crystals

MDPI

Article

Mixed Convective Radiative Flow through a Slender Revolution Bodies Containing Molybdenum-Disulfide Graphene Oxide along with Generalized Hybrid Nanoparticles in Porous Media

Umair Khan [1], Aurang Zaib [2,3,*], Mohsen Sheikholeslami [4], Abderrahim Wakif [5] and Dumitru Baleanu [6,7,8]

1 Department of Mathematics and Social Sciences, Sukkur IBA University, Sukkur 65200, Sindh, Pakistan; umairkhan@iba-suk.edu.pk
2 Department of Natural Sciences, The Begum Nusrat Bhutto Women University, Sukkur 65170, Pakistan
3 Department of Mathematical Sciences, Federal Urdu University of Arts, Science & Technology, Gulshan-e-Iqbal, Karachi 75300, Pakistan
4 Department of Mechanical Engineering, Babol Noshiravni University of Technology, P.O. Box 484, Babol, Mazandaran, Iran; mohsen.sheikholeslami@yahoo.com
5 Laboratory of Mechanics, Faculty of Sciences Aïn Chock, Hassan II University, B.P. 5366 Mâarif, Casablanca 20100, Morocco; wakif.abderrahim@gmail.com
6 Department of Mathematics, Cankaya University, Ankara 06790, Turkey; dumitru.baleanu@gmail.com
7 Institute of Space Sciences, 077125 Magurele, Romania
8 Department of Medical Research, China Medical University, Taichung 40447, Taiwan
* Correspondence: aurangzaib@fuuast.edu.pk

Received: 29 July 2020; Accepted: 28 August 2020; Published: 31 August 2020

Abstract: The current framework tackles the buoyancy flow via a slender revolution bodies comprising Molybdenum-Disulfide Graphene Oxide generalized hybrid nanofluid embedded in a porous medium. The impact of radiation is also provoked. The outcomes are presented in this analysis to examine the behavior of hybrid nanofluid flow (HNANF) through the cone, the paraboloid, and the cylinder-shaped bodies. The opposing flow (OPPF) as well as the assisting flow (ASSF) is discussed. The leading flow equations of generalized hybrid nanoliquid are worked out numerically by utilizing bvp4c solver. This sort of the problem may meet in the automatic industries connected to geothermal and geophysical applications where the sheet heat transport occurs. The impacts of engaging controlled parameters of the transmuted system on the drag force and the velocity profile are presented through the graphs and tables. The achieved outcomes suggest that the velocity upsurges due to the dimensionless radius of the slender body parameter in case of the assisting flow and declines in the opposing flow. Additionally, an increment is observed owing to the shaped bodies as well as in type A nanofluid and type B hybrid nanofluid.

Keywords: hybrid nanofluid; slender body revolution; porous media; radiation effect; mixed convection

1. Introduction

The research regarding the convective-flow entrenched in porous media widely has been utilized owing to its vast engineering applications as solar collectors, heat exchangers, post-accidental heat exclusion in nuclear reactors, building construction, drying processes, oil recovery and geothermal, ground water pollution, etc. Nield [1] analyzed the liquid flow of stability ensuing through a vertical mass and thermal gradients via a horizontal-layer immersed in porous media. Bejan and Khair [2]

explored the marvel of mass and heat transfer through a vertical sheet entrenched in a porous medium and they have taken unvarying concentration as well as temperature. The impact of mixed as well as free convective flows with heat transport through a slender revolution of the body in a porous medium was examined by Lai et al. [3] and they concluded that the temperature gradient shrinks due to dimensional radius. The thermal and mass diffusion through a cone embedded in porous medium was scrutinized by Yih [4]. Bano and Singh [5] explored the radiation influence on mass and heat transport from a radiated thin needle in a saturated porous medium by utilizing a technique of Von Karman-integral. Singh and Chandarki [6] inspected the free convective flow with mass and heat transfer through a vertical cylinder occupied in porous media. The mixed convective flow through a vertical flat surface in a porous medium with nanoliquid was examined by Ahmad and Pop [7]. Talebizadeh et al. [8] scrutinized the impact of radiation on natural convective flow through a porous vertical surface and found numerical as well as exact solutions. Moghimi et al. [9] discussed the MHD (magnetohydrodynamic) influence on natural convective flow via a sphere saturated in a porous medium. Moghimi et al. [10] obtained an exact solution of flow through a flat surface with constant heat flux and slip effect by utilizing DQM (differential quadrature method) and HAM (homotopy analysis method). Raju and Sandeep [11] inspected the magnetic influence on flow of mass and heat transport containing Casson fluid through a rotated vertical cone/plate in porous media with micro-organisms. They perceived that the mass and heat transfer from a cone is superior compared to flow over a plate. Raju et al. [12] applied the Buongiorno model to inspect the phenomenon of mass and heat transport through a radiated revolution slender body in porous media. They perceived that the behavior of temperature shrinks in a flow revolution over a cone compared to flow revolution through the cylinder and paraboloid.

Several recent explorations divulged that nanofluids have superior capability of heat transport than convectional fluids. Thus, it is likely to swap conventional heat transport fluids via nanofluids in the numerous designs of heat transport like heat exchanger, heat generators, and cooling systems. Choi [13] observed that, by scattering metallic nanometer sized particles in regular heat transport liquids, the ensuing nanoliquids hold greater thermal conductivity than those of presently utilized ones. Further, Eastman et al. [14] discovered that the shape of the particle has a stronger effect on nanofluid effective thermal conductivity than the size of particle or thermal conductivity of the particle. To augment the nanofluids heat transport owing to nanoparticles migration and the resulting boundary-layer disturbance was experimentally examined by Wen and Ding [15]. The Boltzmann technique to inspect the magnetic impact on the natural convective flow comprising nanoliquid through a cylindrical annulus was studied by Ashorynejad et al. [16]. The impact of distinct shapes of nanoscale particles in EG (entropy generation) based aqueous solution was inspected by Ellahi et al. [17]. Inspired by the importance of nanofluids, several researchers recently were engaged with the debate of flow with heat transport to nanoliquids via different perspective [18–21].

Recently, a novel type of fluid, suggested hybrid nanofluids has been utilized to augment the heat transport in applications of thermal [22–24]. Hybrid nanoliquids consist of two or more different nanoparticles in either mixture of non-composite forms. Hybrid nanofluids envisages in the fields of heat transport as electronic and generator cooling, thermal storage, biomedical, cooling of transformer, lubrication, solar heating, spacecraft and aircraft, welding, protection, refrigeration, and heat pump. Minea [25] inspected the estimations of distinct viscosity of hybrid nanoliquid by scattering the water-based TiO_2, Al_2O_3, and SiO_2 nanomaterials. The impact of nonlinear radiation on the magneto flow of micropolar hybrid (Cu-Al_2O_3) dusty nanofluid from a stretched sheet was examined by Ghadikolaei et al. [26]. Sheikoleslami et al. [27] scrutinized the modeling of the porous domain with Lorentz forces and radiation impact and obtained the solution by CVFEM (control volume based finite element method). They explored that temperature gradient has greater influence due to the greater buoyancy parameter. Gholinia et al. [28] inspected the steady magneto flow of hybrid CNTs (carbon nanotubes) nanofluid over a permeable stretched cylinder. Recently, Khan et al. [29]

discussed the influence of magnetic function comprising ethylene glycol-based hybrid nanofluid from a stretched/shrinking wedge with mixed convection and stability analysis performed.

The earlier review literature reveals that the mixed convective generalized hybrid (MoS_2-Go) nanofluid flow through a slender revolution bodies in porous media has been highlighted as a mostly unknown area. The radiation impact with generalized hybrid single phase model is discussed here, which is not considered in the earlier published results [7,11]. The leading PDEs (partial differential equations) are altered into ODEs (ordinary differential equation) through suitable transformations and then tackled via three stage Lobatto formula. Impacts of the pertinent variables are portrayed and investigated through the graphs.

2. Problem Formulation

In the current exploration, the buoyancy flow through a slender revolution bodies containing Molybdenum-Disulfide Graphene Oxide along with the generalized hybrid nanofluid entrenched in a saturated porous medium is shown schematically in Figure 1. To optimize the heat transport, the impact of radiation in the occurrence of the opposing and the assisting flows is analyzed. It is assumed that the ambient velocity is considered as $u_e(x) = U_\infty x^m$ with constant U_∞, while T_∞ the constant free stream temperature. The temperature of the slender revolution body is taken as $T_w(x)$ with $T_w(x) > T_\infty$ utilizes for (ASSF) and $T_w(x) < T_\infty$ uses for (OPPF). The system of coordinate from the slender body vortex is at origin, while the distance along the revolution body and normal to the slender revolution body is presented by the cylindrical coordinate (x, r). Applying the single-phase model suggested by the Tiwari and Das [30] with the approximations of Boussinesq and boundary layer scaling, the leading equations are

$$\frac{\partial(ru)}{\partial x} + \frac{\partial(vr)}{\partial r} = 0 \tag{1}$$

$$\frac{\mu_{HNF}}{\mu_F}\frac{\partial u}{\partial r} = \frac{Kg(\rho\beta)_F}{\mu_F}\frac{(\rho\beta)_{HNF}}{(\rho\beta)_F}\frac{\partial T}{\partial r} \tag{2}$$

$$u\frac{\partial T}{\partial x} + v\frac{\partial T}{\partial r} = \frac{k_{HNF}}{\left(\rho c_p\right)_{HNF} r}\frac{\partial}{\partial r}\left(r\frac{\partial T}{\partial r}\right) - \frac{1}{\left(\rho c_p\right)_{HNF}}\frac{\partial}{\partial r}(rq_r) \tag{3}$$

with the corresponding boundary conditions

$$\begin{array}{l} v = 0,\ T = T_w(x) = T_\infty + \mathrm{A}x^\lambda \text{ at } r = R(x), \\ u = u_e(x) = U_\infty x^m,\ T = T_\infty \text{ as } r \to \infty. \end{array} \tag{4}$$

Integrating Equation (2) and utilizing Equation (4), it becomes

$$\frac{\mu_{HNF}}{\mu_F}u = \frac{\mu_{HNF}}{\mu_F}u_e + \frac{Kg\beta_F}{\nu_F}\frac{(\rho\beta)_{HNF}}{(\rho\beta)_F}(T - T_\infty) \tag{5}$$

Here v, u signify Darcy's law velocity components in (r, x) directions, T temperature of the hybrid nanofluid, g acceleration owing to gravity, μ_{HNF} hybrid viscosity, μ_F base fluid viscosity, K permeability of the porous medium, k_{HNF} hybrid nanofluid thermal conductivity, $\left(\rho c_p\right)_{HNF}$ hybrid nanofluid heat capacitance, $(\rho\beta)_{HNF}$ hybrid nanofluid thermal expansion, and $R(x)$ surface shape of the axisymmetric body.

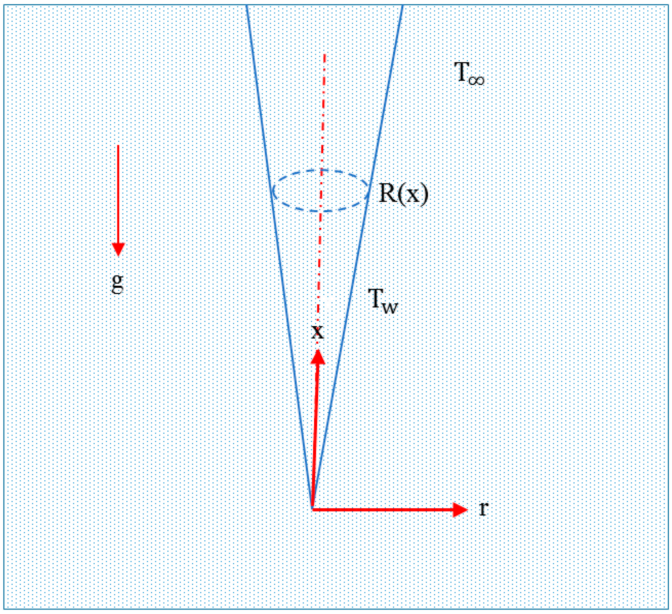

Figure 1. Physical diagram of the problem.

For radiation effect, the Rosseland approximation is illustrated as

$$q_r = -\frac{4\gamma_1}{3k_1}\left(\frac{\partial T^4}{\partial r}\right) \tag{6}$$

where k_1 and γ_1 signify coefficient of mean absorption and Stefan–Boltzmann, respectively. Applying Taylor series to expand T^4 about T_∞ and prohibiting the terms involving higher-order, one gets

$$T^4 \cong 4TT_\infty^3 - 3T_\infty^4 \tag{7}$$

The similarity variables for further analysis are introduced as

$$\begin{gathered}\psi = \alpha_F x F(\eta),\ \eta = Pe_x\frac{r^2}{x^2} = \frac{U_\infty r^2 x^{m-1}}{\alpha_F},\ \theta(\eta) = (T - T_\infty)/(T_w - T_\infty),\\ Pe_x = \frac{U_\infty x^{m+1}}{\alpha_F},\ u = 2u_e F',\ v = \frac{\alpha_F}{r}\eta(1-m)F' - \frac{\alpha_F}{r}F,\ R_d = \frac{4\gamma_1 T_\infty^3}{k_1 k_F}.\end{gathered} \tag{8}$$

Equation (1) is identically true and Equation (3) and Equation (5) are transformed to

$$\frac{\mu_{HNF}}{\mu_F}(2F' - 1) - \frac{Kg\beta_F x^{\lambda-m}}{\nu_F U_\infty}\frac{(\rho\beta)_{HNF}}{(\rho\beta)_F}\theta = 0 \tag{9}$$

$$\left(\frac{k_{HNF}}{k_F} + \frac{4}{3}R_d\right)(2\eta\theta'' + 2\theta') + \frac{\left(\rho c_p\right)_{HNF}}{\left(\rho c_p\right)_F}(\theta' F - \lambda F'\theta) = 0 \tag{10}$$

It is perceptible that Equation (9) and Equation (10) will consent the similarity solutions if the power of x in Equation (9) disappears, i.e.,:

$$m = \lambda \tag{11}$$

With this classified condition, Equation (9) can be rewritten as

$$\frac{\mu_{HNF}}{\mu_F}(2F' - 1) - \xi\frac{(\rho\beta)_{HNF}}{(\rho\beta)_F}\theta = 0 \tag{12}$$

where the dimensionless constraint involved in the aforementioned equations is mathematically expressed as

$$\xi = \frac{Ra}{Pe_x} = \frac{Kg\beta_F(T_w - T_\infty)x}{\nu_F\alpha_F}\frac{\alpha_F}{U_\infty x^{m+1}} = \frac{Kg\beta_F A}{\nu_F U_\infty},\ Ra = \frac{Kg\beta_F(T_w - T_\infty)x}{\nu_F\alpha_F},$$
$$Pe_x = \frac{U_\infty x^{m+1}}{\alpha_F},\ \mathrm{Pr} = \frac{\nu_F}{\alpha_F},\ R_d = \frac{4\gamma_1 T_\infty^3}{k_1 k_F}.$$

and the interpretation of these constraints are the mixed convection parameter, the local Rayleigh number for a porous medium, the Peclet number, the Prandtl number and the radiation parameter, respectively.

Placing $\eta = b$, where b is constant and utilized for a slender body, it is numerically small. Equation (9) stipulated the body size as well as body shape with surface is defined via

$$R(x) = \left(\frac{\nu_F\alpha_F bRa}{Pe_x Kg\beta_F A}\right)^{\frac{1}{2}} x^{(\frac{1-\lambda}{2})}\ \mathrm{OR}\left(\frac{b}{Pe_x}\right)^{\frac{1}{2}} x \tag{13}$$

The problems concerning the realistic interest, the amount of $\lambda \leq 1$. For instance, $\lambda = 1$, $\lambda = 0$ and $\lambda = -1$ represent the cylinder, paraboloid, and cone shape bodies.

The boundary restrictions are

$$\begin{gathered} b(1-m)F' - F = 0,\ \theta = 1 \text{ at } \eta = b, \\ F' \to 0.5,\ \theta \to 0 \text{ as } \eta \to \infty. \end{gathered} \tag{14}$$

If Equation (10) and Equation (12) are merged, one gets

$$\left(\frac{k_{HNF}}{k_F} + \frac{4}{3}R_d\right)(4\eta F''' + 4F'') + \frac{\left(\rho c_p\right)_{HNF}}{\left(\rho c_p\right)_F}\left(2FF'' - 2\lambda F'^2 + \lambda F'\right) = 0 \tag{15}$$

along with the modified boundary restrictions

$$b(1-m)F'(b) - F(b) = 0,\ \frac{\mu_{HNF}}{\mu_F}(2F'(b) - 1) = \xi\frac{(\rho\beta)_{HNF}}{(\rho\beta)_F},\ F'(\infty) \to 0.5. \tag{16}$$

The quantities of practical interest and to measure the liquid behaviors is the skin friction which is explained as

$$C_F = \frac{\tau_w}{\rho u_e^2} = \frac{\mu_{HNF}\left.\frac{\partial u}{\partial r}\right|_{r=R(x)}}{\rho u_e^2} \tag{17}$$

The skin friction in the dimensional form is

$$\frac{Pe_x^{0.5}}{\mathrm{Pr}}C_F = 4\frac{\mu_{HNF}}{\mu_F}b^{\frac{1}{2}}F''(b). \tag{18}$$

3. Model of Generalized Hybrid Nanoliquid

In numerical and experimental investigations on the behaviors of nanofluid, modeling their physical quantities using condensed mathematical relationships between solid particles and regular liquid is a common procedure. Numerous experiments have been performed to validate such terms for nanofluids dilute in scattering of a single sort of solid material [31] and mixtures of two kinds of particles (Suresh et al. [32]). Devi and Devi [33] recommended a collection of correlation for hybrid nanofluid physical-quantities. They approached the liquid involving a single sort of nanoparticle as the regular liquid and the other sort of nanoparticle as the individual particle. The relationship of thermal conductivity and viscosity matched Suresh et al.'s [32] experimental outcomes. In the approach of Devi and Devi [33], there exists the non-linear terms owing to the communication of two sorts of distinct nanoparticles. However, in dilute mixtures where the volumetric fractions of nanoparticle are generally tiny, the impacts of these non-linear conditions may not be important. Thus, it realistically ignores the non-linear terms in the model of Devi and Devi. The hybrid nanofluid model in simplified form and the models of normal nanofluid and Devi and Devi are scheduled in Table 1, where Type A signifies the conventional nanoliquid model, Types B and C, respectively; indicate the hybrid nanoliquid model of Devi and Devi and the model of hybrid nanoliquid in simplified form. Devi and Devi [33] used the approach of the recurrence formulae to signify the density, viscosity, thermal conductivity, and specific heat of the hybrid nanoliquid related generally to the N-th type of nanoparticles as

$$\rho_{HNF} \equiv \rho_{HNF_N} = (1-\phi_N)\rho_{HNF_{N-1}} + \phi_N \rho_{S_N} \tag{19}$$

$$\mu_{HNF} \equiv \mu_{HNF_N} = \frac{\rho_{HNF_{N-1}}}{(1-\phi_N)^{2.5}} \tag{20}$$

$$k_{HNF} \equiv k_{HNF_N} = \frac{k_{S_N} + k_{HNF_{N-1}}(M-1) - \phi_N(M-1)\left(k_{HNF_{N-1}} - k_{S_N}\right)}{k_{S_N} + k_{HNF_{N-1}}(M-1) + \phi_N\left(k_{HNF_{N-1}} - k_{S_N}\right)} \tag{21}$$

$$\left(\rho c_p\right)_{HNF} \equiv \left(\rho c_p\right)_{HNF_N} = \phi_N\left(\rho c_p\right)_{S_N} + (1-\phi_N)\left(\rho c_p\right)_{HNF_{N-1}} \tag{22}$$

$$\beta_{HNF} \equiv \beta_{HNF_N} = (1-\phi_N)\beta_{HNF_{N-1}} + \phi_N \beta_{S_N} \tag{23}$$

From the above correlations, ignoring the non-linear terms, one obtains

$$\rho_{HNF} = 1 - \rho_F \sum_{a=1}^{N} \phi_a + \sum_{a=1}^{N} \phi_a \rho_{S_a} \tag{24}$$

$$\mu_{HNF} = \frac{\mu_F}{\left(1 - \sum\limits_{a=1}^{N} \phi_a\right)^{2.5}} \tag{25}$$

$$\left(\rho c_p\right)_{HNF} = 1 - \left(\rho c_p\right)_F \sum_{a=1}^{N} \phi_a + \sum_{a=1}^{N} \phi_a \left(\rho c_p\right)_{S_a} \tag{26}$$

$$\beta_{HNF} = 1 - \beta_F \sum_{a=1}^{N} \phi_a + \sum_{a=1}^{N} \phi_a \beta_{S_a} \tag{27}$$

It is worth mentioning that for k_{HNF}, we remain the recurrence Formula (21) because of the connections amid dissimilar particles can barely be uttered by the Maxwell equations. Additionally, throughout the research the values of $M = 3$ is taken which implies that the shape of the particle is spherical.

Table 1. Thermo-physical models of nanofluid and hybrid nanofluid.

Property	Types	Correlation
Density	A	$\rho_{NF} = (1-\phi)\rho_F + \phi\rho_S$
	B	$\rho_{HNF} = (1-\phi_2)\left[(1-\phi_1)\rho_F + \phi_1\rho_{S_1}\right] + \phi_2\rho_{S_2}$
	C	$\rho_{HNF} = (1-\phi_1-\phi_2)\rho_F + \phi_1\rho_{S_1} + \phi_2\rho_{S_2}$
Viscosity	A	$\mu_{NF} = \frac{\mu_F}{(1-\phi)^{2.5}}$
	B	$\mu_{HNF} = \frac{\mu_F}{(1-\phi_1)^{2.5}(1-\phi_2)^{2.5}}$
	C	$\mu_{HNF} = \frac{\mu_F}{(1-\phi_1-\phi_2)^{2.5}}$
Heat Capacity	A	$\left(\rho c_p\right)_{NF} = (1-\phi)\left(\rho c_p\right)_F + \phi\left(\rho c_p\right)_S$
	B	$\left(\rho c_p\right)_{HNF} = (1-\phi_2)\left[(1-\phi_1)\left(\rho c_p\right)_F + \phi_1\left(\rho c_p\right)_{S_1}\right] + \phi_2\left(\rho c_p\right)_{S_2}$
	C	$\left(\rho c_p\right)_{HNF} = (1-\phi_1-\phi_2)\left(\rho c_p\right)_F + \phi_1\left(\rho c_p\right)_{S_1} + \phi_2\left(\rho c_p\right)_{S_2}$
Thermal conductivity	A	$k_{NF} = \frac{k_S + (M-1)k_F - (M-1)\phi(k_F - k_S)}{k_S + (M-1)k_F + \phi(k_F - k_S)}$
	B & C	$k_{HNF} = \frac{k_{S_2} + (M-1)k_{MF} - (M-1)\phi_2\left(k_{MF} - k_{S_2}\right)}{k_{S_2} + (M-1)k_{MF} + \phi_2\left(k_{MF} - k_{S_2}\right)}$ where $k_{MF} = \frac{k_{S_1} + (M-1)k_F - (M-1)\phi_1\left(k_F - k_{S_1}\right)}{k_{S_1} + (M-1)k_F + \phi_1\left(k_F - k_{S_1}\right)}k_F$
Thermal expansion	A	$\beta_{NF} = (1-\phi)\beta_F + \phi\beta_S$
	B	$\beta_{HNF} = (1-\phi_2)\left[(1-\phi_1)\beta_F + \phi_1\beta_{S_1}\right] + \phi_2\beta_{S_2}$
	C	$\beta_{HNF} = (1-\phi_1-\phi_2)\beta_F + \phi_1\beta_{S_1} + \phi_2\beta_{S_2}$
Pr	6.2	-	-

4. Results and Discussion

The primary intention is to scrutinize the characteristics of generalized hybrid nanoliquid for the mixed convective flow comprising MoS_2-Go nanoparticles through slender revolution bodies. The non-linear Equation (15) with boundary restrictions (Equation (16)) has been worked out numerically via Lobatto IIIa formula. The thickness of the boundary layer is considered as 30 for convergence of profiles asymptotically which is essential for this type of problem. Table 2 represents the thermo-physical characteristics of the base and nanofluids. The outcomes of the sundry parameters in the presence of the water-based fluid and the type B hybrid nanofluid on the field of velocity distribution and the skin friction have been examined in Figures 2–13. For validation, the results of the current problem have been compared with the outcomes of Ahmad et al. [34] and Saleh et al. [35] as shown in Table 3. An excellent harmony is seen. Whereas the numerical values of types B and C hybrid nanofluid for (ASSF) as well as for (OPPF) are displayed in Tables 4 and 5.

Table 2. Thermo-physical properties of the base fluid and hybrid nanoparticles.

Characteristic Properties	H_2O	MoS_2	GO
ρ	997.1	5060	1800
c_p	4179	397.21	717
k	0.613	904.4	5000
β	21	2.8424×10^{-5}	2.84×10^{-4}

Table 3. Comparison values of $F''(b)$ when $m = 1,\ \lambda = 0,\ \xi = -1,\ R_d = \phi = 0,\ \mathrm{Pr} = 1$ for the distinct values of b.

b	Ahmed et al. [34]	Saleh et al. [35]	Current
0.01	8.4924360	8.4924452	8.4924456
0.1	1.2888171	1.2888299	1.28883009

Table 4. Computation of the $\mathrm{Pr}^{-1}Pe_x^{0.5}C_F$ for the assisting flow $\xi = 1.1$ utilizing the two different types of models varying ϕ_2 while the other fixed parameters are $m = \lambda = 1,\ b = 0.1,\ R_d = 0.5$.

ϕ_1	ϕ_2	Type B	Type C
0.025	0.025	−2.3995	−2.3973
	0.030	−2.3760	−2.3733
	0.035	−2.3527	−2.3496
0.030	0.025	−2.3754	−2.3727
	0.030	−2.3522	−2.3490
	0.035	−2.3292	−2.3255
0.035	0.025	−2.3516	−2.3485
	0.030	−2.3287	−2.3250
	0.035	−2.3060	−2.3017

Table 5. Computation of the $\mathrm{Pr}^{-1}Pe_x^{0.5}C_F$ for the opposing flow $\xi = -1.1$ utilizing the two different types of models varying ϕ_2 while the other fixed parameters are $m = \lambda = 1,\ b = 0.1,\ R_d = 0.5$.

ϕ_1	ϕ_2	Type B	Type C
0.025	0.025	1.9037	1.9031
	0.030	1.8954	1.8946
	0.035	1.8869	1.8859
0.030	0.025	1.8951	1.8943
	0.030	1.8866	1.8856
	0.035	1.8779	1.8767
0.035	0.025	1.8862	1.8853
	0.030	1.8776	1.8764
	0.035	1.8688	1.8673

The outcomes, indicating from these tables the type B hybrid nanofluid, are superior to the type C hybrid nanofluid. Moreover, in case of the assisting flow, the skin friction increases by 0.979% for the type B hybrid nanofluid whereas the skin friction in the type C hybrid nanofluid augments by 1.001%. As the value of the nanoparticle volumetric fraction increases, the skin friction decreases continuously for both types of hybrid nanofluid. In contrast, the skin friction decreases up to 0.435%

for the type B hybrid nanofluid due to the fixed value of the parameter $\phi_2 = 0.025$ in the example of opposing flow while for the type C hybrid nanofluid, it is decreased by 0.446%. Due to very small negligible differences in the outcomes of both the types of hybrid nanofluid, therefore the computation throughout the paper is done only for the type B hybrid nanofluid.

Figures 2 and 7 are set to inspect the impact of the dimensionless radius of the slender body parameter b and the volume fraction of nanoparticle ϕ_2 on the velocity gradient against the similarity variable η for the three different phenomena such as the assisting and opposing flows, shape bodies and the normal nanofluid as well for the hybrid nanofluid. In the example of assisting flow, the velocity distribution and the momentum boundary-layer flow (MBLF) increase with increasing the dimensionless radius of the slender body parameter b, while in the phenomenon of the opposing flow, the behavior of the motion of the fluid behaves in the contrary direction as shown in Figure 2. It is transparent to observe from the outcomes that the gap between the curves is initially more significant in the ASSF as well as in the OPPF, while as we upsurge, the value of the dimensionless radius of the slender body parameter b the gap between the solution curves is reduced.

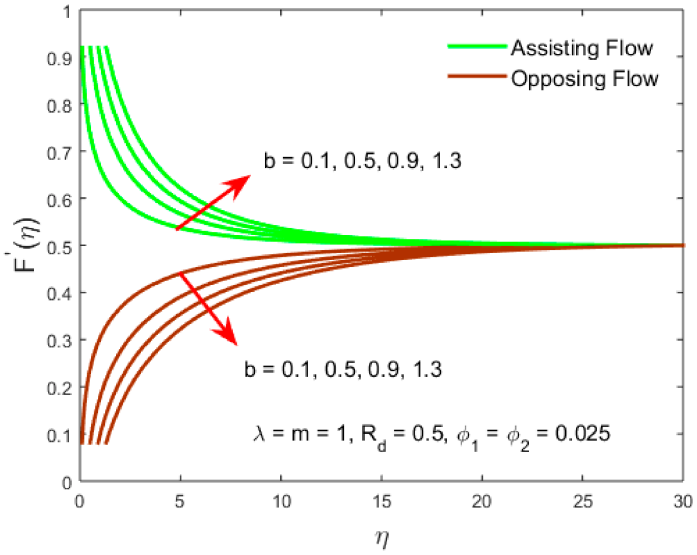

Figure 2. The variation of the velocity profile $F'(\eta)$ for the case of assisting and opposing flow versus the similarity variable η for the distinct values of the dimensionless radius of the slender body parameter b.

On the other hand, the velocity distribution is enhancing the function of the shape bodies as well as for the type B hybrid nanofluid and the type A nanofluid for the higher values of b as shown in Figures 3 and 4, respectively. It is perceived from Figure 3 that the velocity field is superior in the flow through a cone compared to paraboloid and cylindrical type's bodies. Moreover, it is perfectly visible from the graph that the liquid flow accelerates more for the MoS_2/water nanoparticle or type A nanofluid as compared to the type B hybrid nanoparticles as highlighted in Figure 4. The gap between the solution curves in the shape bodies is more when compared to the solution curves like Figure 4. Since Figure 5, it has been noticed that for the (ASSF), the velocity distribution decreases with escalating ϕ_2, whereas for the opposing flow, it is augmented.

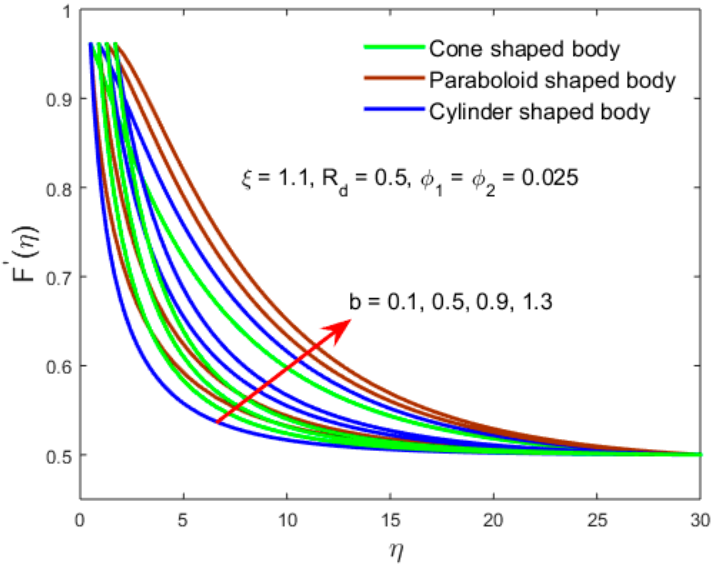

Figure 3. The variation of the velocity profile $F'(\eta)$ for the three important cases of shape bodies such as Cone, paraboloid, and cylinder versus the similarity variable η for the distinct values of the dimensionless radius of the slender body parameter b.

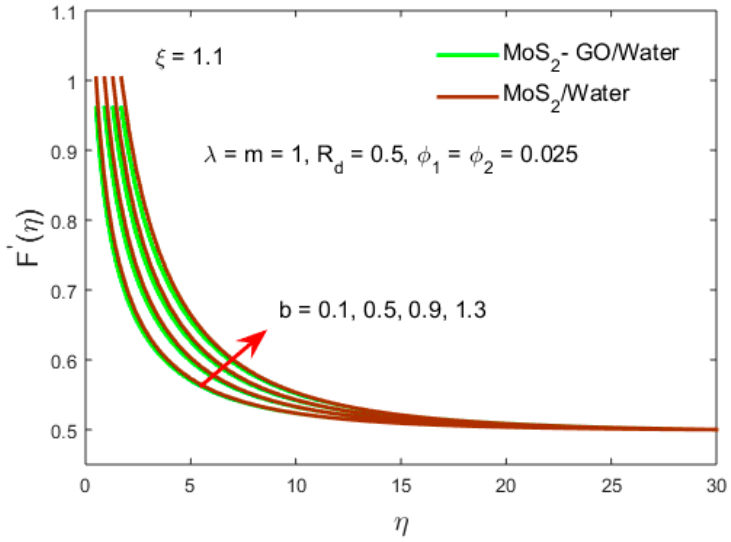

Figure 4. The variation of the velocity profile $F'(\eta)$ for the type A normal nanofluid as well as for the type B hybrid nanofluid versus the similarity variable η for the distinct values of the dimensionless radius of the slender body parameter b.

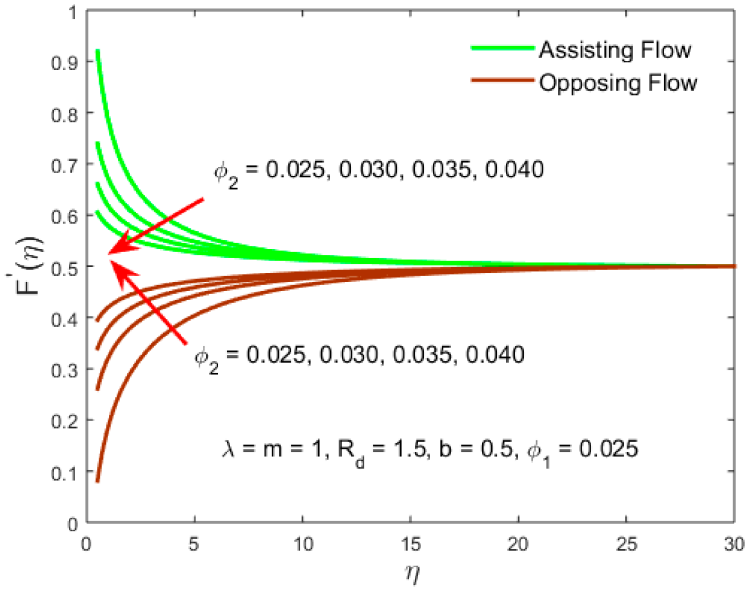

Figure 5. Shows the variation of the velocity profile $F'(\eta)$ for the case of assisting and opposing flow versus the similarity variable η for the distinct values of the volume fraction of nanoparticle ϕ_2.

Additionally, it explains that the thickness of the velocity and the (MBLF) declines with ϕ_2 for the ASSF and augments for the OPPF. The outcome of the velocity gradient in Figure 5 is showing a contrary behavior in both the cases of ASSF and OPPF as we compare with the solution curves of Figure 2. From Figure 6, it is transparent that due to the shape bodies, the velocity field is decelerated for the higher impact of ϕ_2. In comparison, the flow of the velocity field over the cone shape body is finer than the rest of the two-shape body. Generally, the velocity upsurges due to the fact that type B hybrid nanofluid dynamic viscosity has an inverse relationship to nanoparticle volume fraction. Hence, an augmenting in ϕ_2 guides to the decline's viscosity of base liquid and therefore speeds up the motion of the liquid flow.

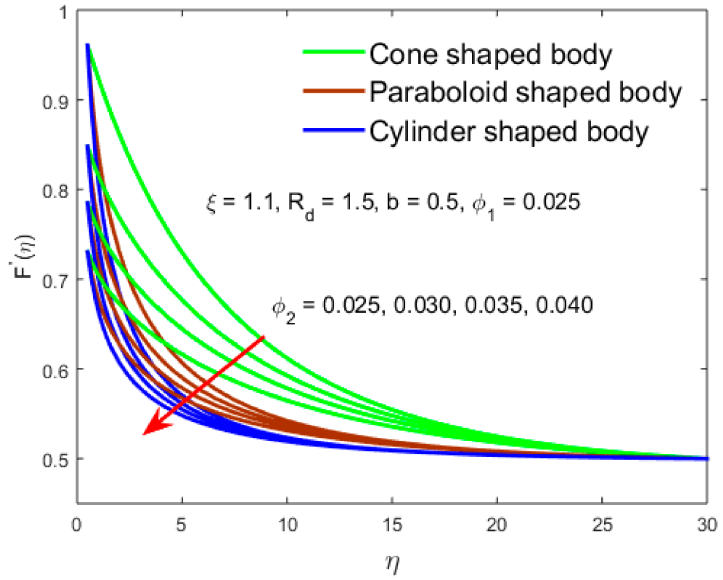

Figure 6. Shows the variation of the velocity profile $F'(\eta)$ for the three important cases of shape bodies such as Cone, paraboloid, and cylinder versus the similarity variable η for the distinct values of the volume fraction of nanoparticle ϕ_2.

Moreover, the velocity profile reduces due to ϕ_2 for the type B hybrid nanofluid and type A nanofluid as portrayed in Figure 7. The impact between the curves is very minor for the parameter ϕ_2 while the outcome for the type B hybrid nanofluid is higher than the type A nanofluid.

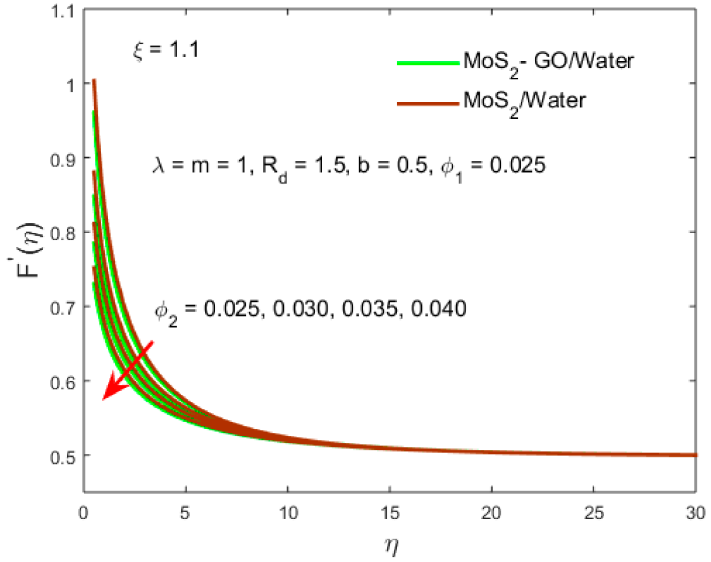

Figure 7. The variation of the velocity profile $F'(\eta)$ for the type A normal nanofluid as well as for the type B hybrid nanofluid versus the similarity variable η for the distinct values of the volume fraction of nanoparticle ϕ_2.

Figures 8 and 9 highlight the stimulus of radiation parameter R_d on the velocity distribution against the similarity variable of the two distinct phenomena such as the assisting and opposing flows as well as for the type A nanofluid and type B hybrid nanofluid. It is clear from Figure 8 as depicted graphically that the velocity distribution augments for the ASSF and declines for the OPPF as the value of the radiation parameter R_d upsurges. The solution behavior is similarly observed like Figure 2 while the contrary behavior of the outcomes in Figure 5 is seen for both the cases ASSF and as well as in the OPPF, while in comparison the influence between the curves is less. Additionally, R_d is exploited to drop the molecules of liquid into hydrogen. Figure 9 displays that the velocity upsurges are owed to magnifying the radiation parameter for the type A nanofluid as well as for the type B hybrid nanofluid. The motion of the fluid flow for the type A nanofluid is superior as compare to the type B hybrid nanofluid. In addition, the solution impact in the curves for the velocity gradient is more owing to the impact of radiation parameter as compared to the significant impact of the other two parameters which is exercised in Figures 4 and 7, respectively.

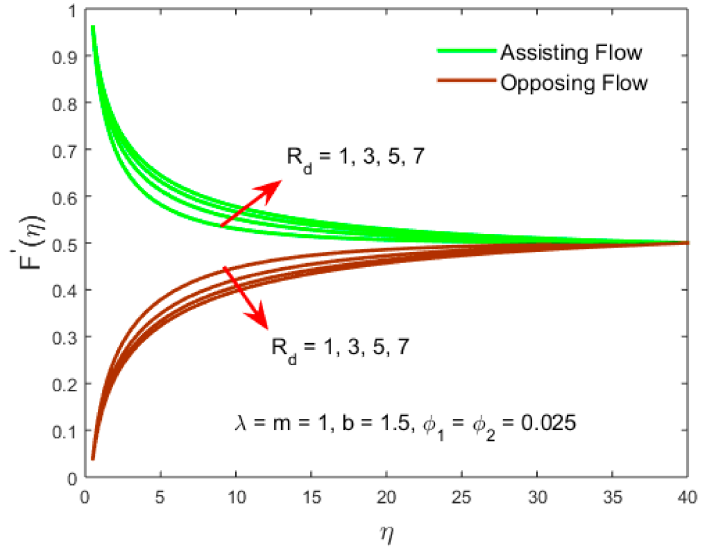

Figure 8. Shows the variation of the velocity profile $F'(\eta)$ for the case of assisting and opposing flow versus the similarity variable η for the distinct values of the radiation parameter R_d.

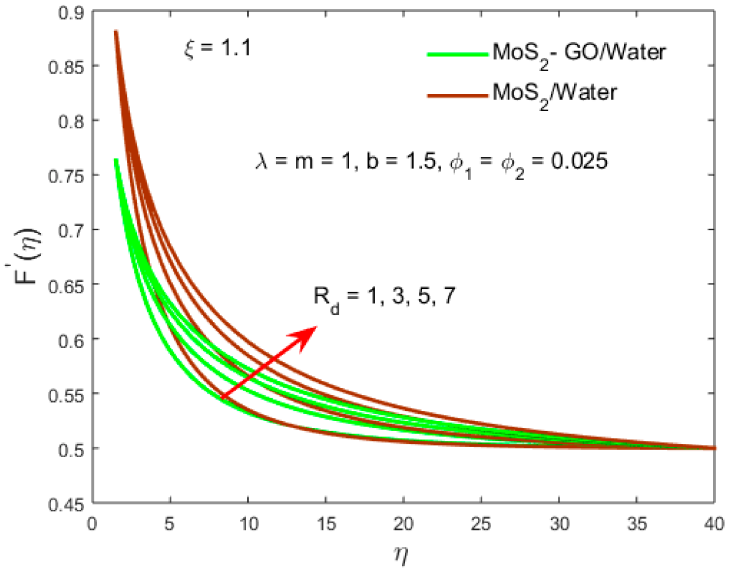

Figure 9. The variation of the velocity profile $F'(\eta)$ for the type A normal nanofluid as well as for the type B hybrid nanofluid versus the similarity variable η for the distinct values of the radiation parameter R_d.

Figures 10–13 show the variation of the dimensionless radius of the slender body parameter b and the nanoparticle volume fraction ϕ_2 on the skin friction against the mixed convection parameter ξ for the two distinct cases such as the flow over the shape bodies and the corresponding type A nanofluid and the type B hybrid nanofluid. The skin friction is reduced with enhanced b along the horizontal axis of the range $(-\infty < \xi \leq 0)$ and augments in the spectrum $(0 \leq \xi < \infty)$ for the flow over the shape bodies as well as for the types A and B nanofluid and hybrid nanofluid as highlighted in Figures 10 and 11, respectively. The skin friction is higher in the range $(0 \leq \xi < \infty)$ for the flow over the cone shape body and also for the type B hybrid nanofluid as compared to the flow on the paraboloid and the cylindrical shape bodies as well as for the type A nanofluid, while the opposite trend is observed in the range $(-\infty < \xi \leq 0)$ as shown in Figures 10 and 11. The range in both graphs is taken from $-0.5 \leq \xi \leq 0.5$ and it is not the fixed one we can vary from this range as a real number $(-\infty < \xi < \infty)$ but due to this

small range in the solution, the collision is more effectively significant. A similar behavior is detected (Figures 10 and 11) for the skin friction owing to the nanoparticle volume fraction ϕ_2 as described in Figures 12 and 13, respectively. Hence, in Figures 12 and 13 illustrate more transparently the impact of the curves of the flow over the shape bodies against the mixed convection parameter owing to b is greater compared to ϕ_2 on the skin friction while this gap for the type B hybrid nanofluid and type A nanofluid owing the parameter ϕ_2 is coarsened as compared to the dimensionless radius of the slender body parameter b.

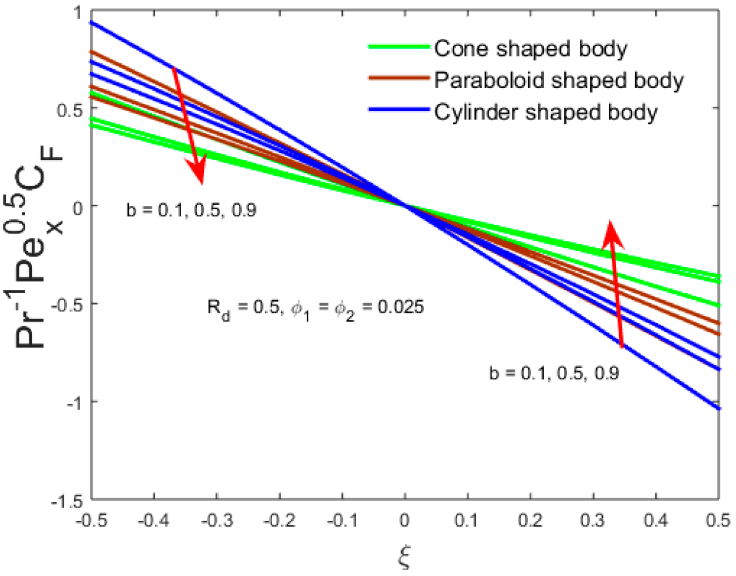

Figure 10. Deviation of the skin friction versus the mixed convection parameter ξ for the distinct values of the dimensionless radius of the slender body parameter b.

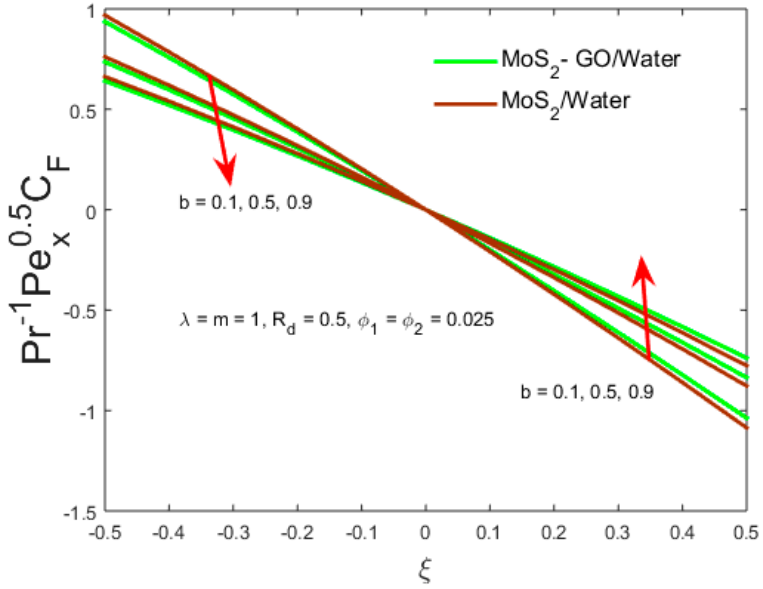

Figure 11. Deviation of the skin friction versus the mixed convection parameter ξ for the distinct values of the dimensionless radius of the slender body parameter b.

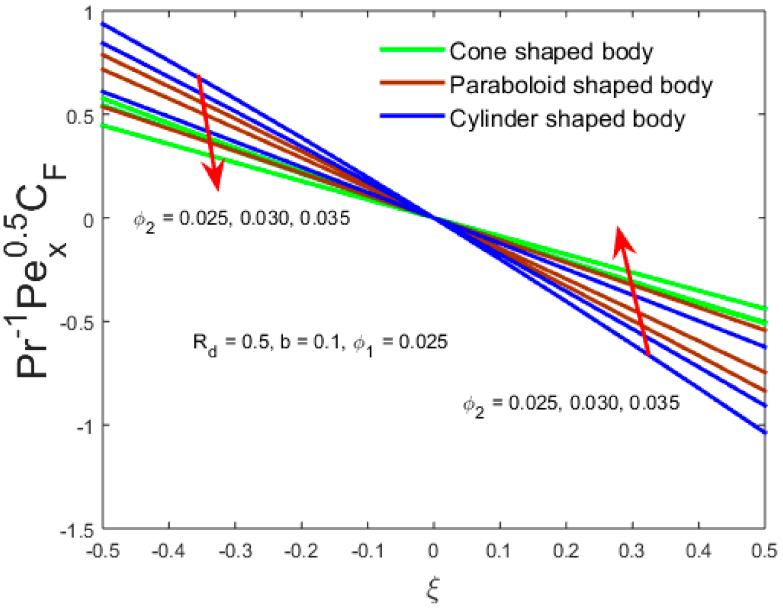

Figure 12. Deviation of the skin friction versus the mixed convection parameter ξ for distinct values of the volume fraction of nanoparticle ϕ_2.

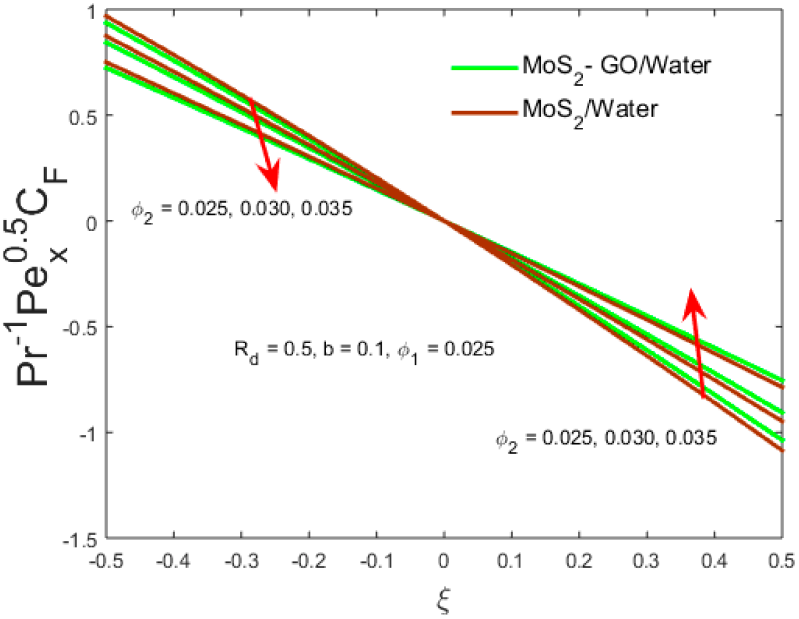

Figure 13. Deviation of the skin friction versus the mixed convection parameter ξ for distinct values of the volume fraction of nanoparticle ϕ_2.

5. Concluding Remarks

The key points of the current study are summarized as:

- The velocity augments for the (ASSF) and declines for the (OPPF) owing to magnifying the dimensionless radius of the slender body parameter b while the change behavior is detected in response of the higher nanoparticle volume fraction ϕ_2.
- The persistent effect of b, the velocity upsurges for the flow of the shape bodies like paraboloid shape body ($\lambda = 0$), cylindrical shape body ($\lambda = 1$) as well as cone shape body ($\lambda = -1$) while the same behavior of the velocity is seen in the type A nanofluid and type B hybrid nanofluid.

- The velocity field decreases for the type A nanofluid as well as for the type B hybrid nanofluid and also for the flow over the different shape bodies owing to ϕ_2.
- Due to R_d, the velocity upsurges for the type A nanofluid as well as for the type B hybrid nanofluid while for the type B hybrid nanofluid, the velocity is lesser relative to the type A nanofluid.
- The skin friction under the distinct shape bodies and along the type A nanofluid and type B hybrid nanofluid are augmented for both parameter b and ϕ_2 along the x-axis of the slender sheet in the range $0 \leq \xi < \infty$ while vice versa in the range $-\infty < \xi \leq 0$.

This sort of problem may be useful in geothermal and geophysical applications. Thus, the outcomes of the problem will be obliging in the evaluation and assessment of resources in geothermal energy.

Author Contributions: Conceptualization, A.Z.; Data curation, A.W.; Formal analysis, M.S.; Investigation, A.W.; Methodology, U.K.; Resources, A.Z.; Software, U.K. and A.Z.; Supervision, D.B. All authors have read and agreed to the published version of the manuscript.

Funding: This research received no external funding.

Conflicts of Interest: The authors declare no conflict of interest.

References

1. Nield, D.A. Onset of Thermohaline Convection in a Porous Medium. *Water Resour. Res.* **1968**, *4*, 553–560. [CrossRef]
2. Bejan, A.; Khair, K.R. Heat and mass transfer by natural convection in a porous medium. *Int. J. Heat Mass Transf.* **1985**, *28*, 909–918. [CrossRef]
3. Lai, F.; Pop, I.; Kulack, F. Free and mixed convection from slender bodies of revolution in porous media. *Int. J. Heat Mass Transf.* **1990**, *33*, 1767–1769. [CrossRef]
4. Yih, K.A. Coupled heat and mass transfer by free convection over a truncated cone in porous media: VWT/VWC or VHF/VMF. *Acta Mech.* **1999**, *137*, 83–97. [CrossRef]
5. Bano, N.; Singh, B.B. An integral treatment for coupled heat and mass transfer by natural convection from a radiating vertical thin needle in a porous medium. *Int. Commun. Heat Mass Transf.* **2017**, *84*, 41–48. [CrossRef]
6. Singh, B.; Chandarki, I. Integral treatment of coupled heat and mass transfer by natural convection from a cylinder in porous media. *Int. Commun. Heat Mass Transf.* **2009**, *36*, 269–273. [CrossRef]
7. Ahmad, S.; Pop, I. Mixed convection boundary layer flow from a vertical flat plate embedded in a porous medium filled with nanofluids. *Int. Commun. Heat Mass Transf.* **2010**, *37*, 987–991. [CrossRef]
8. Talebizadeh, P.; Moghimi, M.A.; Kimiaeifar, A.; Ameri, M. Numerical and analytical solutions for natural convection flow with thermal radiation and mass transfer past a moving vertical porous plate by dqm and ham. *Int. J. Comput. Methods* **2011**, *8*, 611–631. [CrossRef]
9. Moghimi, M.A.; Talebizadeh, P.; Mehrabian, M.A. Heat generation/absorption effects on magnetohydrodynamic natural convection flow over a sphere in a non-Darcian porous medium. *Proc. Inst. Mech. Eng. Part E J. Process. Mech. Eng.* **2010**, *225*, 29–39. [CrossRef]
10. Moghimi, M.A.; Tabaei, H.; Kimiaeifar, A. HAM and DQM solutions for slip flow over a flat plate in the presence of constant heat flux. *Math. Comput. Model.* **2013**, *58*, 1704–1713. [CrossRef]
11. Raju, C.S.K.; Sandeep, N. Heat and mass transfer in MHD non-Newtonian bio-convection flow over a rotating cone/plate with cross diffusion. *J. Mol. Liq.* **2016**, *215*, 115–126. [CrossRef]
12. Raju, C.S.K.; Saleem, S.; Upadhya, S.M.; Hussain, I. Heat and mass transport phenomena of radiated slender body of three revolutions with saturated porous: Buongiorno's model. *Int. J. Therm. Sci.* **2018**, *132*, 309–315. [CrossRef]
13. Choi, S.U.S. Enhancing thermal conductivity of fluids with nanoparticles. In Proceedings of the 1995 International Mechanical Engineering Congress and Exhibition, San Francisco, CA, USA, 12–17 November 1995.
14. Eastman, J.A.; Choi, S.; Li, S.; Yu, W.; Thompson, L.J. Anomalously increased effective thermal conductivities of ethylene glycol-based nanofluids containing copper nanoparticles. *Appl. Phys. Lett.* **2001**, *78*, 718–720. [CrossRef]

15. Wen, D.; Ding, Y. Experimental investigation into convective heat transfer of nanofluids at the entrance region under laminar flow conditions. *Int. J. Heat Mass Transf.* **2004**, *47*, 5181–5188. [CrossRef]
16. Ashorynejad, H.R.; Mohamad, A.A.; Sheikholeslami, M. Magnetic field effects on natural convection flow of a nanofluid in a horizontal cylindrical annulus using Lattice Boltzmann method. *Int. J. Therm. Sci.* **2013**, *64*, 240–250. [CrossRef]
17. Ellahi, R.; Zeeshan, A.; Hassan, M. Particle shape effects on Marangoni convection boundary layer flow of a nanofluid. *Int. J. Numer. Methods Heat Fluid Flow* **2016**, *26*, 2160–2174. [CrossRef]
18. Soomro, F.A.; Zaib, A.; Haq, R.U.; Sheikholeslami, M. Dual nature solution of water functionalized copper nanoparticles along a permeable shrinking cylinder: FDM approach. *Int. J. Heat Mass Transf.* **2019**, *129*, 1242–1249. [CrossRef]
19. Tabassum, R.; Mehmood, R. Crosswise stream of methanol–iron oxide (CH3OH–Fe_3O_4) with temperature-dependent viscosity and suction/injection effects. *Proc. Inst. Mech. Eng. Part E: J. Process. Mech. Eng.* **2019**, *233*, 1013–1023. [CrossRef]
20. Zaib, A.; Khan, U.; Wakif, A.; Zaydan, M. Numerical Entropic Analysis of Mixed MHD Convective Flows from a Non-Isothermal Vertical Flat Plate for Radiative Tangent Hyperbolic Blood Biofluids Conveying Magnetite Ferroparticles: Dual Similarity Solutions. *Arab. J. Sci. Eng.* **2020**, *45*, 5311–5330. [CrossRef]
21. Sayed, A.Y.; Abdel-Wahed, M.S. Entropy analysis for an MHD nanofluid with a microrotation boundary layer over a moving permeable plate. *Eur. Phys. J. Plus* **2020**, *135*, 1–17. [CrossRef]
22. Alsarraf, J.; Rahmani, R.; Shahsavar, A.; Afrand, M.; Wongwises, S.; Tran, M.D. Effect of magnetic field on laminar forced convective heat transfer of MWCNT–Fe_3O_4/water hybrid nanofluid in a heated tube. *J. Therm. Anal. Calorim.* **2019**, *137*, 1809–1825. [CrossRef]
23. Shahsavar, A.; Sardari, P.T.; Toghraie, D. Free convection heat transfer and entropy generation analysis of water–Fe_3O_4/CNT hybrid nanofluid in a concentric annulus. *Int. J. Numer. Methods Heat Fluid Flow* **2019**, *29*, 915–934. [CrossRef]
24. Khan, U.; Shafiq, A.; Zaib, A.; Baleanu, D. Hybrid nanofluid on mixed convective radiative flow from an irregular variably thick moving surface with convex and concave effects. *Case Stud. Therm. Eng.* **2020**, *21*, 100660. [CrossRef]
25. Minea, A.A. Hybrid nanofluids based on Al_2O_3, TiO_2 and SiO_2: Numerical evaluation of different approaches. *Int. J. Heat Mass Transf.* **2017**, *104*, 852–860. [CrossRef]
26. Ghadikolaei, S.; Hosseinzadeh, K.; Hatami, M.; Ganji, D. MHD boundary layer analysis for micropolar dusty fluid containing Hybrid nanoparticles (Cu-Al2O3) over a porous medium. *J. Mol. Liq.* **2018**, *268*, 813–823. [CrossRef]
27. Sheikholeslami, M.; Gerdroodbary, M.B.; Shafee, A.; Tlili, I. Hybrid nanoparticles dispersion into water inside a porous wavy tank involving magnetic force. *J. Therm. Anal. Calorim.* **2019**, 1–7. [CrossRef]
28. Gholinia, M.; Armin, M.; Ranjbar, A.; Ganji, D. Numerical thermal study on CNTs/ $C_2H_6O_2$– H_2O hybrid base nanofluid upon a porous stretching cylinder under impact of magnetic source. *Case Stud. Therm. Eng.* **2019**, *14*, 100490. [CrossRef]
29. Khan, U.; Zaib, A.; Mebarek-Oudina, F. Mixed Convective Magneto Flow of SiO_2–MoS_2/$C_2H_6O_2$ Hybrid Nanoliquids Through a Vertical Stretching/Shrinking Wedge: Stability Analysis. *Arab. J. Sci. Eng.* **2020**, 1–13. [CrossRef]
30. Tiwari, R.K.; Das, M.K. Heat transfer augmentation in a two-sided lid-driven differentially heated square cavity utilizing nanofluids. *Int. J. Heat Mass Transf.* **2007**, *50*, 2002–2018. [CrossRef]
31. Pak, B.C.; Cho, Y.I. Hydrodynamic and heat transfer study of dispersed fluids with submicron metallic oxide particles. *Exp. Heat Transf.* **1998**, *11*, 151–170. [CrossRef]
32. Suresh, S.; Venkitaraj, K.; Selvakumar, P.; Chandrasekar, M. Synthesis of Al_2O_3–Cu/water hybrid nanofluids using two step method and its thermo physical properties. *Colloids Surfaces A: Physicochem. Eng. Asp.* **2011**, *388*, 41–48. [CrossRef]
33. Devi, S.S.U.; Devi, S.A. Numerical investigation of three-dimensional hybrid Cu–Al_2O_3/water nanofluid flow over a stretching sheet with effecting Lorentz force subject to Newtonian heating. *Can. J. Phys.* **2016**, *94*, 490–496. [CrossRef]

34. Ahmad, R.; Mustafa, M.; Hina, S. Buongiorno's model for fluid flow around a moving thin needle in a flowing nanofluid: A numerical study. *Chin. J. Phys.* **2017**, *55*, 1264–1274. [CrossRef]
35. Salleh, S.N.A.; Bachok, N.; Arifin, N.M.; Ali, F.M.; Pop, I. Magnetohydrodynamics Flow Past a Moving Vertical Thin Needle in a Nanofluid with Stability Analysis. *Energies* **2018**, *11*, 3297. [CrossRef]